Int. J. Electrochem. Sci., 9 **(2014)** 5280 - 5288

International Journal of
ELECTROCHEMICAL
SCIENCE
www.electrochemsci.org

Short communication

Synthesis of Single Crystalline Spinel $LiMn_2O_4$ Nanorods for a Lithium Ion Battery

Zhang Kai[*], *Wei Yang, Zong Shuang, Yu Yan, Ping Hao, Li Guiwei, Jia Jianli*

School of Chemical and Environmental Engineering, China University of Mining and Technology, (Beijing), Beijing, 100083, PR China
[*]E-mail: zhangkaicumtb@sina.com

Received: 17 April 2014 / *Accepted:* 25 May 2014 / *Published:* 16 June 2014

Single crystalline $LiMn_2O_4$ nanorod was synthesized by solid state reaction at 650 ºC using γ-MnOOH nanorod as a self-template, which is obtained by a typical hydrothermal process. X-ray diffraction, scanning electron microscopy, transmission electron microscopy and electrochemical tests were thoroughly investigated. The results show that $LiMn_2O_4$-650 have good discharge capacity, cycle stability and rate performance. $LiMn_2O_4$-650 sample delivers initial discharge capacity of 102 mAh/g and retains 90 mAh/g after 100 cycles at 5 C rate. The probable effect of structure and prepared-temperature is detailed analyzed.

Keywords: MnOOH; $LiMn_2O_4$; Nanorod; Cathode materials; Lithium-ion battery.

1. INTRODUCTION

The electric vehicle (EV) using a rechargeable lithium ion battery is seen as one of the ways to solve two great problems of industry: the shortage of oil energy sources and the pollution of the environment. Rechargeable lithium-ion batteries have been enjoying a significant commercial success as the most promising energy source in the electric vehicle mainly by their high working voltages, high energy density, long life etc. Currently, $LiCoO_2$, $LiNiO_2$ and $LiMn_2O_4$ are the main cathode materials for rechargeable lithium-ion batteries[1-3]. Among these, spinel $LiMn_2O_4$ has been extensively studied as one of the most promising cathode material for LIBs because of its intrinsic low-cost, environmental friendliness, high abundance, better safety and facile production[4, 5]. $LiMn_2O_4$ electrodesin the 4 V (versus Li/Li^+) region suffer fromcapacity fading especially at elevated temperature (50-60°C). The capacity loss has been ascribed to several factors such as i) Jahn-Teller distortion due to Mn^{3+} ions, ii)

the dissolution of manganese ions into the electrolyte, iii) loss of crystallinity during cycling and iv) electrolyte decomposition at the high potential regions [6-8].Therefore, much effort was devoted previously to resolving these problems such as stabilization of spinel structure b y sol–gel method [9], Pechini process [10], combustion [11] and chemical precipitation [12]. Although uniform $LiMn_2O_4$ particles with good electrochemical performance could be thus obtained, the synthetic procedures are generally complex and costly. Moreover nanostructured lithium intercalated compounds with various morphologies have been extensively prepared to improve their rate capability for lithium ion batteries due to present the favorable plane of Li^+ ions diffusion: for instance, nanoparticles, nanowires, nanotubes, hollow spheres and mesoporous materials [13-16] and so on. Indeed, such an improvement is often considered to be achieved at the expense of high volumetric energy density, but high volumetric energy density and high power are often incompatible requirement. Therefore, to synthesize high power capable nanosized materials, it is highly recommended to develop a simple and scalable method like the solid state reaction route.

In the study, γ-MnOOH which has a particular one-dimensional structure was considered as a possible precursor to produce $LiMn_2O_4$ nanosized cathode material for Li-ion battery, effective approach in order to reduce the side reactions at the interface between the cathode electrode and electrolyte. Although the grain size distribution of the lithiated phase and maintaining the γ-MnOOH precursor nanorod morphology during phase transformation is a formidable challenge, chemical lithiation of transition metal oxides has been reported to enhance the performance of a Li-ion battery without significant change of oxide morphology [17, 18]. In this paper, we successfully synthesized spinel $LiMn_2O_4$ nanorods using a facile, easy to scale up two-step process: a hytrothermal reaction to prepare γ-MnOOH nanorods followed by solid state reaction with LiOH. To understand the rate capability of the $LiMn_2O_4$ synthesized at 650 ºC, structure and morphology were also investigated and its mechanism is also discussed in detail.

2. EXPERIMENTAL

The synthesis of γ-MnOOH was carried out via one-step hydrothermal method. The stoichiometric amount of $MnSO_4 \cdot H_2O$, $KMnO_4$ and CTAB (Hexadecyl trimethyl ammonium bromide) was mixed well in distilled water and stirred for an hour. Afterwards, the suspension was transferred into a 100 mL Teflon-lined stainless-steel autoclave, sealed and maintained at 160 ºC for 25 h. The product was cooled to room temperature, filtered and washed with distilled water, ethanol and acetone. Finally, the brown powder were obtained and dried under vacuum at 60 ºC for 10 h[19].

$LiMn_2O_4$ powder was prepared by the following procedure: A stoichiometrically required amount of as-prepared γ-MnOOH was added to an aqueous solution of $LiOH \cdot H_2O$ and stirred for an hour. The mixture was heated to dryness then the solid product was ground and calcinated in air at 650 ºC for 15 h, respectively. The final products were referred to as "$LiMn_2O_4$-650".

X-ray diffraction (XRD, Rigaku D/Max-2400, Japan) using Cu Kα radiation was employed to identify the crystalline phase of the synthesized material. The data were recorded in the 10-80° 2θ range at the scanning rate of 6°/min. The patterns were analyzed by the Rietveld method as

implemented in the program GSAS. Scanning electron microscopy (SEM, Hitachi S-4800, Japan), transmission electron microscopy (TEM) and high-resolution transmission electron microscopy (HR-TEM, JEOL-2100F, Japan) were engaged to observe morphology, size and distribution of as-prepared composites.

The electrodes were fabricated by casting a slurry of 75 wt.% active material, 15 wt.% carbon black, and 10 wt.% poly(vinylidene fluoride) (PVDF) in *N*-methylpyrrolidinone (NMP) solvent onto an Al foil substrate. The slurry was dried in vacuum at 60 °C overnight. The film was cut into pieces of about 0.6×0.6 cm^2 to act as electrodes. The testing half-cells were assembled in an Ar-filled glove box (MB-10-G with TP170b/mono, MBRAUN) with lithium metal as counter and reference electrode. Electrolyte was 1M $LiPF_6$ in a mixed solution of Ethylene carbonate (EC) and Diethyl carbonate (DEC) (1:1 in volume ratio). The charge-discharge measurements were galvanostatically carried out using a battery test system (NEWARE BTS-610, Newware Technology Co., Ltd., China) at different current density in the voltage range of 2.0-4.6V (vs. Li/Li^+). Cyclic voltammograms (CVs) were measured on an electrochemical workstation (CHI1100A) at a scan rate of 0.1mVs^{-1} between 3.6 and 4.5V (vs. Li/Li^+).

3. RESULTS AND DISCUSSION

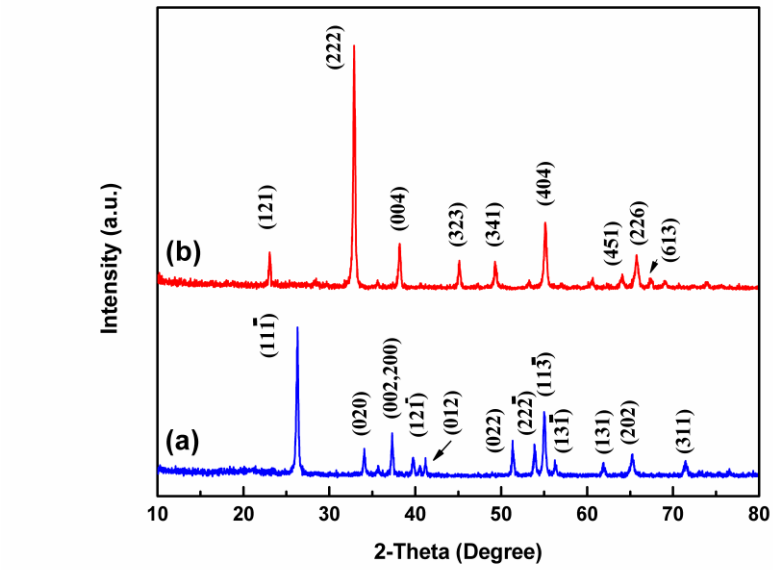

Figure 1. (a) XRD patterns for the γ-MnOOH nanorods prepared by hydrothermal at 160 ºC. (b) XRD patterns of the β-Mn_2O_3 nanorods prepared by calcination of γ-MnOOH nanorods at 350 ºC for 1h.

Figure 1 shows XRD patterns of nanostructure γ-MnOOH and β-Mn_2O_3. All the peaks in the Fig.1a can be indexed to a monoclinic phase (JCPDS No. 41-1379) with lattice constants a=5.300Å, b=5.278Å and c=5.307Å. Fig.2a shows the SEM image of as-prepared γ-MnOOH nanorods. It is can

be observed that large quantity of uniform rod-like nanostructures with about 200-300 nm in width and approximately 8 μm in length. The rod-like nanostructure of the γ-MnOOH is calcined at 350ºC for 1h. Fig.1b the 2Φ of sample at 23.92º, 32.76º, 38.06º, 49.15º, 55.00º, 65.62º correspond to the characteristic peaks, respectively, of the β-Mn_2O_3 (JCPDS No.24-0508). It indicates its nanorods almost unchanged after calcined in Fig.2b.

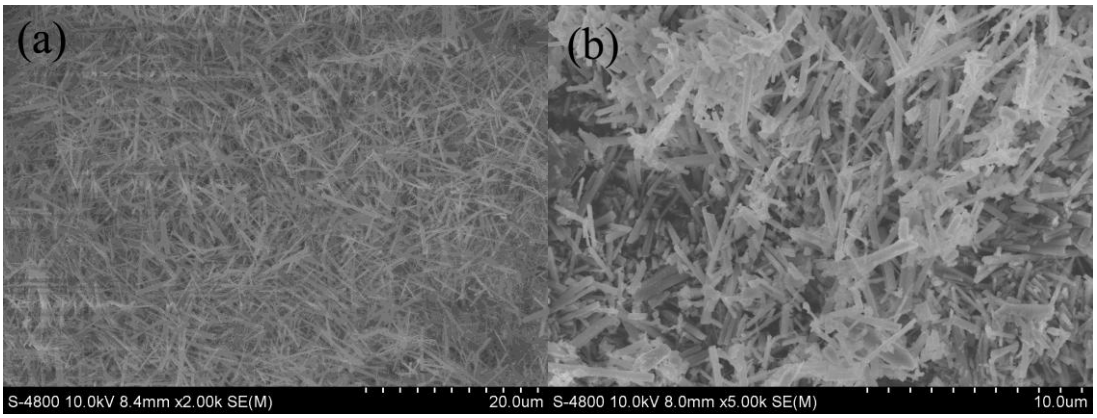

Figure 2. SEM images of the precursors: (a) γ-MnOOH nanorods; (b) β-Mn_2O_3 nanorods.

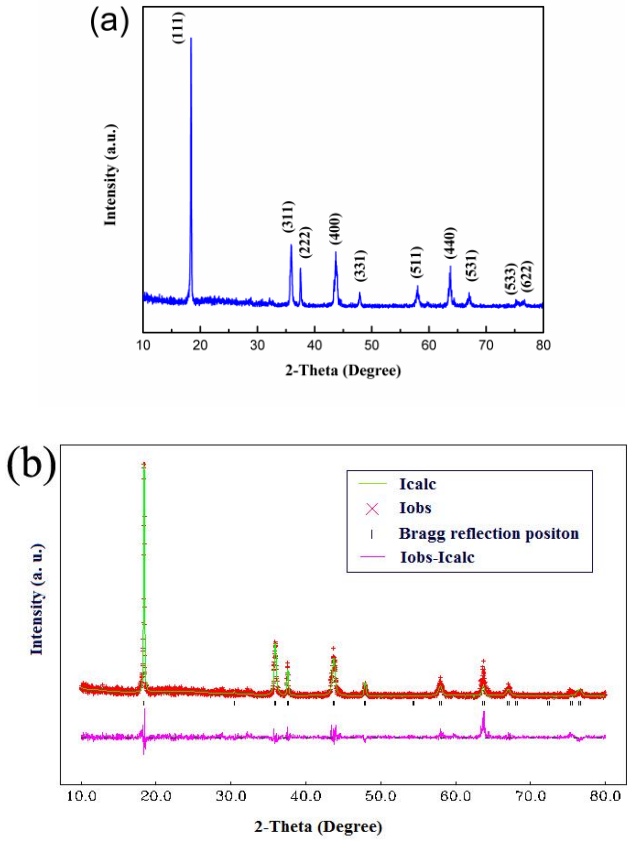

Figure 3. (a) XRD pattern of the $LiMn_2O_4$ nanorods; (b) Rietveld refinement of XRD pattern of the $LiMn_2O_4$ nanorods.

Figure 3 shows XRD patterns and the Rietveld refinement profiles of the $LiMn_2O_4$ precursors calcined at 650 ºC for 15h in air. All the peaks can be indexed to a pure cubic spinel phase (Fd3m, space group 227) which corresponds to JCPDS data No.35-0782, shown in Fig.3a. No peaks of γ-MnOOH precursor phase and other impurities were detected. The peak intensity is intensive. It is implied that the crystallinity of $LiMn_2O_4$-650 sample is good. The data for the samples obtained at 650 ºC were listed in table 1.

Table 1. Cell parameters data for the cubic spinel $LiMn_2O_4$ samples obtained at 650

Sample		**$LiMn_2O_4$-650**
a(Å)		8.235
V(Å^3)		558.556
Plane(400)/degree	Position/2θ	43.72
	FWHM	0.40

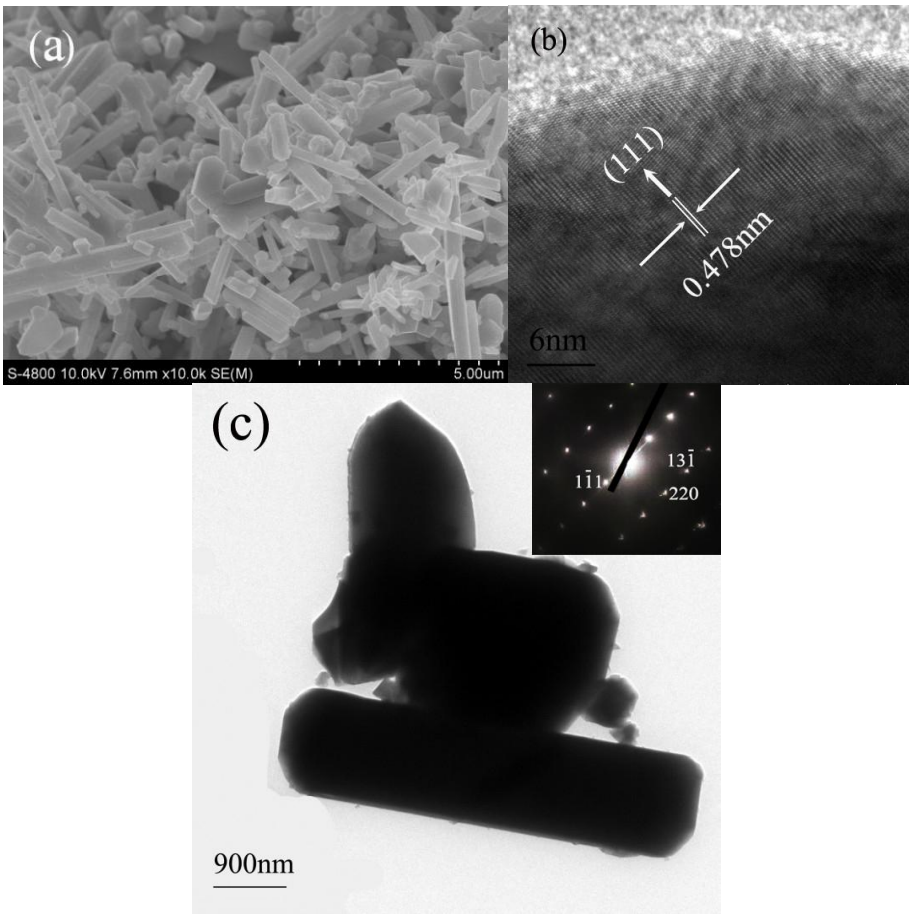

Figure 4. SEM, TEM, HRTEM and SAED images of $LiMn_2O_4$ nanorods obtained at 650 ºC; (a, b, c).

The cell parameters, the position and full width at half maximum (FWHM) of the (400)-plane peak are the important factors for the crystallinity of spinel structure, reported by Manev et al. [20] and Lee et al. [21]. According to table 1, $LiMn_2O_4$-650 displayed good crystallinity. It is also a significant factor of electrochemical performance for cathode materials. The lattice parameter value of $LiMn_2O_4$-

650 sample is the closed to the critical lattice parameter values of 8.23 Å[22]. The synthesis procedure could be described as follows:

$2MnOOH + O_2 = Mn_2O_3 + H_2O$ (1)

$4LiOH + 4Mn_2O_3 + O_2 = 4LiMn_2O_4 + 2H_2O$ (2)

Figure 4 shows SEM, TEM, HRTEM and SAED images of $LiMn_2O_4$ nanorods obtained at 650 ºC. As can be seen from SEM images (Fig.4a), the $LiMn_2O_4$-650 has the width of 800-900nm and the length of 500nm-5μm, and the slight agglomeration can be observed. $LiMn_2O_4$-650 was well dispersed and maintained the morphology of γ-MnOOH nanorods self-template, in spite of shorter in length to the varying degree, which undergoes an irreversible phase transition [23]. It is probably due to high-temperature process. $LiMn_2O_4$-650 has a three-dimensional lithium diffusion path and every plane is suitable to exchange lithium ion from active materials to the electrolyte, attribute to favorable spinel cubic structure. Generally, it is favorable to shorten the path of intercalation/deintercalation for lithium ion to some extent, thus increasing the actual specific capacity. Rod-like nanostructure of the sample was further examined by TEM and HR-TEM. The HR-TEM images (Fig.4b-4c) show that the sample is single crystalline and match with cubic structure. The diffraction spots can be indexed to (1-11), (13-1) and (220) planes of cubic spinel $LiMn_2O_4$ (JCPDS data No.35-0782). Apparently, the in situ formed $LiMn_2O_4$-650 presents irregular-shaped particles and micron-sized agglomerates.

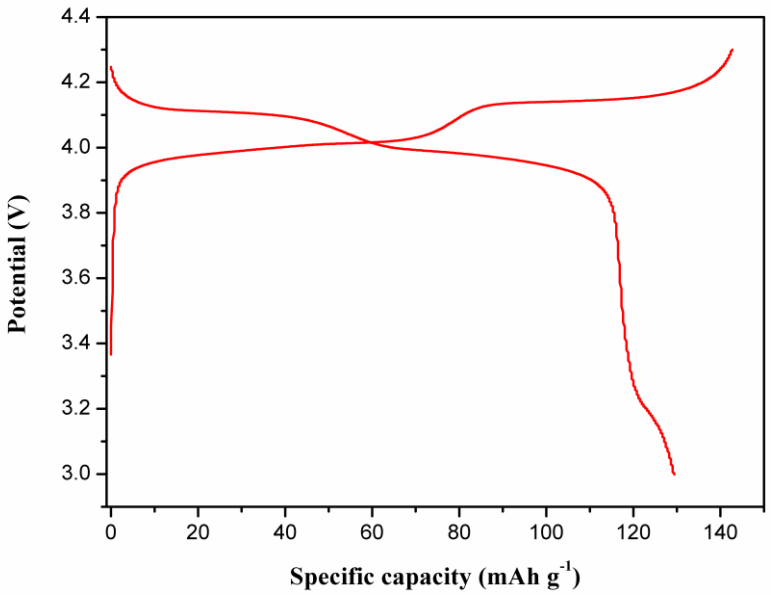

Figure 5. Initial charge-discharge curves of $LiMn_2O_4$-650 in the range of 3.0-4.3V (vs. Li/Li^+) at 0.1C.

Figure 5 shows the initial charge-discharge curves of the sample $LiMn_2O_4$-650 at 0.1C (1C=148 mAh/g). All the samples exhibit two plateaus around 3.95 and 4.18V, due to two-step oxidation/reduction process of spinel $LiMn_2O_4$ [24]. The initial charge and discharge specific capacity of $LiMn_2O_4$-650 sample are 140.2 mAh/g and 129.5 mAh/g respectively, with a columbic efficiency of 92.3%. The decline of columbic efficiency is probably owing to agglomeration of the grains caused by the process of much higher temperature sintering. It maybe reduces specific surface area of the sample

and blocks the full penetration of electrolyte, and thereby cuts down the quantity of intercalation/deintercalation for lithium ion.

Cyclic voltammograms test was engaged to analyze oxidation/reduction and phase transformation processes in electrode reactions [25–27]. Figure 6 depicts the CV curves measured in the potential range of 3.6-4.5V at a sweep rate of 0.1mVs^{-1}. The CV curves exhibit two pairs of clearly separated oxidation/reduction peaks, consistent well with the results shown in Figure 5. The higher oxidation/reduction peaks attribute to Li^+ intercalation/deintercalation from the 8a sites where Li-Li interactions do not occur, corresponding to Li^+ intercalation/deintercalation over the x value range of $0 \le x \le 0.5$ in $Li_xMn_2O_4$. The lower ones are owing to Li^+ intercalation/deintercalation from the 8a sites but where Li–Li interactions occur, corresponding to Li^+ intercalation/deintercalation over the x value range of $0.5 \le x \le 1$ in $Li_xMn_2O_4$ [28]. Table 2 shows the experimental data of the ratio of peak currents (I_{pa}/I_{pc}) and potential interval between oxidation peak and reduction peak ($\Delta\phi_p$). The experimental data of I_{pa}/I_{pc} and $\Delta\phi_p$ for the $LiMn_2O_4$-650 sample are 1.62 and 134 mV. It demonstrates that lithium ions are intercalated and deintercalated reversibly in the $LiMn_2O_4$-650 sample, just as the literature [29].

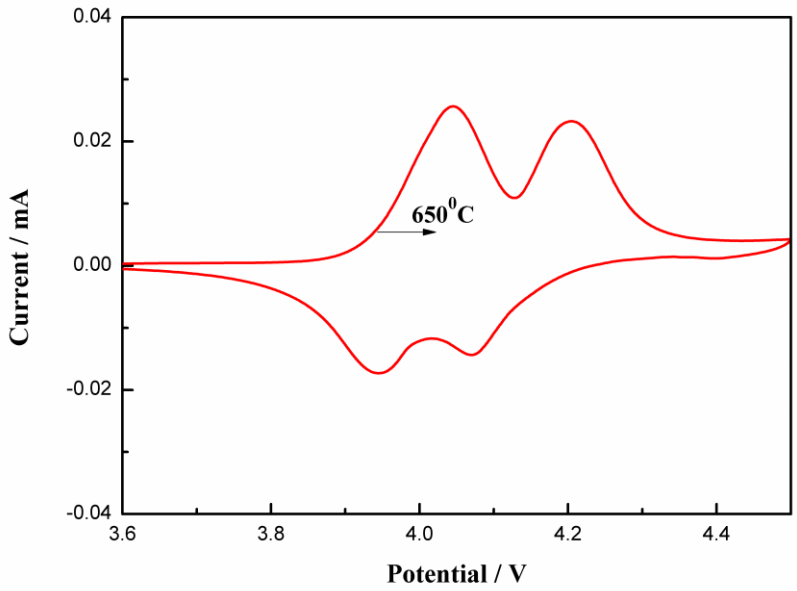

Figure 6. Cyclic voltammograms curves of the $LiMn_2O_4$-650 samples.

Table 2. the experimental data of the ratio of peak currents (I_{pa}/I_{pc}) and potential interval between oxidation peak and reduction peak ($\Delta\phi_p$)

Samples	ϕ_{pa}(V)	ϕ_{pc} (V)	$\Delta\phi_p$ (mV)	I_{pa} (mA)	I_{pc} (mA)	I_{pa}/I_{pc}
$LiMn_2O_4$-650	4.204	4.07	134	0.0233	0.0144	1.62

Figure 7a shows the cycling stability curves for $LiMn_2O_4$-650 samples at varying rates in the potential range of 3.0-4.3V. The discharge capacity of the $LiMn_2O_4$-650 sample remains stable and decreases regularly as the rate increases. Moreover, the capacity can be approximately recovered when

the current density is returned to 0.1C rate. It is implied that the sample own good electrochemical reversibility and cycle stability. Figure 7b shows cycling stability of $LiMn_2O_4$-650 at a 5C rate in the potential range of 3.0-4.3V. The initial irreversible capacity loss of $LiMn_2O_4$-650 is 3.1%, caused by the formation of solid electrolyte interphase (SEI) layer [24].

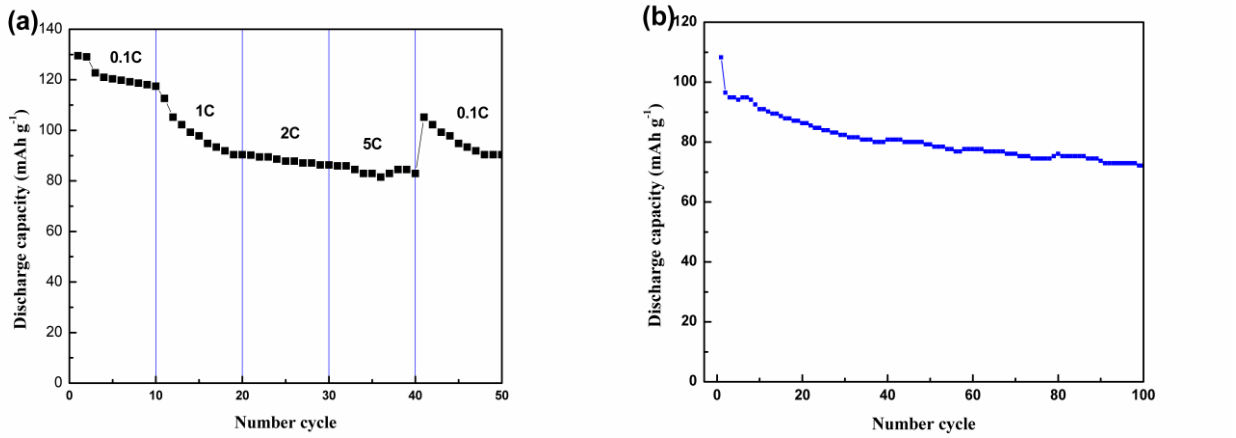

Figure 7. Cycling stability curves of $LiMn_2O_4$-650 sample (a) at varying rates in the potential range of 3.0-4.3V and (b) at a 5C rate in the potential range of 3.0-4.3V.

After the first cycle, the $LiMn_2O_4$-650 sample exhibits excellent cycling performance. It shows a quite slow capacity fading with an average capacity loss of 0.2 mAh/g per cycle during 100 charge-discharge cycles, in other words, the discharge capacity of $LiMn_2O_4$-650 maintains above 83% of its second capacity after 100 cycles.

4. CONCLUSIONS

The single crystalline $LiMn_2O_4$ nanorods have been successfully prepared by solid state reaction using γ-MnOOH nanorod as a self-template at 650 ℃. The results of the electrochemical performance show that $LiMn_2O_4$-650 have good discharge capacity, cycle stability and rate performance. After 100 cycles, $LiMn_2O_4$-650 sample still maintains 90 mAh/g. The sample exhibit high capacity, excellent cycling stability and rate performance. It is meaningful to research high performance spinel $LiMn_2O_4$ as promising substitute of cathode materials for novel lithium ion battery in application.

ACKNOWLEDGEMENTS
This study was supported by a grant from Major State Basic Research Development Program of China (973 Program)(No.2014CB238906).

References

1. G.G. Amatucci, N. Pereira, T. Zheng, I. Plitz, J.M. Tarascon, *J. Power Sources* 81-82(1999) 39.

2. Y.W. Tsai, R. Santhanam, B.J. Hwang, S.K. Hu, H.S. Sheu, *J. Power Sources* 119-121(2003) 701.
3. S.S. Zhang, K. Xu, T.R. Jow, *J. Electrochem. Soc.* 149 (2002) A1521.
4. J.M. Tarascon, W.R. McKinnon, F. Coowar, T.N. Bowmer, G. Amatucci, D. Guyomard, *J. Electrochem. Soc.*141 (1994) 1421–1431.
5. N.J. Dudney, J.B. Bates, R.A. Zuhr, S. Young, J.D. Robertson, H.P. Jun, S.A. Hackney, *J. Electrochem. Soc.* 146(1999) 2455-2464.
6. R.J. Cummow, A. de. Kock, M.M. Thackeray, *Solid State Ionics* 69 (1994) 59.
7. B. Ebin, V. Battaglia, S. Gürmen, *Ceram. Int.* 40 (2014) 7029-7035.
8. Y.K. Sun, D.W. Kim, Y.M. Choi, *J. Power Sources* 79 (1999) 231.
9. C.J. Curtis, J.X.Wang, D.L. Schulz, *J. Electrochem. Soc.* 151 (2004) 590–598.
10. S.H. Wu, H.L. Chen, *J. Power Sources* 119–121 (2003) 134-138.
11. K. Du, H. Zhang, *J. Alloys Compd.* 352 (2003) 250–254.
12. A.R. Naghash, J.Y. Lee, *J. Power Sources* 85 (2000) 284-293.
13. T. Doi, Y. Iriyama, T. Abe, Z. Ogumi, *Chem. Mater.* 17 (2005) 1580-1582.
14. E. Hosono, T. Kudo, I. Honma, H. Matsuda, H. Zhou, *Nano Lett.* 9 (2009) 1045-1051.
15. Y.L. Ding, J. Xie, G.S. Cao, T.J. Zhu, H.M. Yu, X.B. Zhao, *Adv. Funct. Mater.* 21 (2011) 348–355.
16. J.Y. Luo, H.M. Xiong, Y.Y. Xia, *J. Phys. Chem. C* 112 (2008) 12051–12057.
17. B. Garcia, M. Millet, J.P. Pereira-Ramos, N. Baffier, D. Bloch, *J. Power Sources* 81-82 (1999) 670–674.
18. L. Mai, B. Hu, W. Chen, Y. Qi, C. Lao, R. Yang, Y. Dai, Z.L. Wang, *Adv. Mater.* 19 (2007) 3712–3716.
19. L. He, S.C. Zhang, X. Wei, Z. Du, G. Liu, Y. Xing, *J. Power Sources* 220 (2012) 228-235.
20. V. Manev, T. Faulkner, J. Engel, Proc. HBC98, *The First Hawaii Battery Conference*, 1998, p.228.
21. Y.S. Lee, N.J. Kumada, M.Yoshio, *J. Power Sources* 96 (2001) 376.
22. Fábio A. Amaral, Nerilso Bocchi, Ricardo F. Brocenschi, Sonia R. Biaggio, Romeu C. Rocha-Filho, *J. Power Sources* 195 (2010) 3293–3299.
23. D. Linden, T.B. Reddy, In Handbook of Batteries, 3rded. McGraw-Hill: New York (2002) 2.1-2.37.
24. Y.G. Guo, J.S. Hu, L.J. Wan, *Adv. Mater.* 20 (2008) 2878–2887.
25. N. Ding, J. Xu, Y.X. Yao, G. Wegner, X. Fang, C.H. Chen, I. Lieberwirth, *Solid State Ionics* 180 (2009) 222-225.
26. S.B. Tang, M.O. Lai, L. Lu, *Mater. Chem. Phys.* 111 (2008) 149-153.
27. X.W. Chen, C. Chen, L.H. Liu, F. Liu, G.H. Qiu, *Solid State Sci.* 31 (2014) 16-23.
28. B.J. Li, Z. Dang, Y. Zhang, Z.S. Song, *Int. J. Electrochem. Sci.* 9 (2014) 3279-3286.
29. D. Zhan, F. Yang, Q.G. Zhang, X.H. Hu, T.Y. Peng *Electrochim. Acta* 129 (2014) 364–372.